Continuous blood cell separation by hydrophoretic filtration†‡

Sungyoung Choi, Seungjeong Song, Chulhee Choi and Je-Kyun Park*

Received 5th April 2007, Accepted 19th July 2007
First published as an Advance Article on the web 10th August 2007
DOI: 10.1039/b705203k

We propose a new hydrophoretic method for continuous blood cell separation using a microfluidic device composed of slanted obstacles and filtration obstacles. The slanted obstacles have a larger height and gap than the particles in order to focus them to a sidewall by hydrophoresis. In the successive structure, the height and gap of the filtration obstacles with a filtration pore are set between the diameters of small and large particles, which defines the critical separation diameter. Accordingly, the particles smaller than the criterion freely pass through the gap and keep their focused position. In contrast, the particles larger than the criterion collide against the filtration obstacle and move into the filtration pore. The microfluidic device was characterized with polystyrene beads with a minimum diameter difference of 7.3%. We completely separated polystyrene microbeads of 9 and 12 μm diameter with a separation resolution of ~6.2. This resolution is increased by 6.4-fold compared with our previous separation method based on hydrophoresis (S. Choi and J.-K. Park, *Lab Chip*, 2007, 7, 890, ref. 1). In the isolation of white blood cells (WBCs) from red blood cells (RBCs), the microfluidic device isolated WBCs with 210-fold enrichment within a short filtration time of ~0.3 s. These results show that the device can be useful for the binary separation of a wide range of biological particles by size. The hydrophoretic filtration as a sample preparation unit offers potential for a power-free cell sorter to be integrated into disposable lab-on-a-chip devices.

Introduction

Blood is a very complex mixture containing red blood cells (RBCs), white blood cells (WBCs), platelets, and blood plasma proteins. For the proteomic or genomic analysis of WBCs or blood plasma proteins, blood samples need to be separated prior to analysis.[2,3] However, RBCs have a similar diameter to WBCs in suspension, even though the thickness of RBCs is less than their diameter. Furthermore, WBCs exist at low concentration in blood samples, typically less than 0.5% of blood cells. Therefore, many analytical devices rely on conventional off-chip separation methods such as centrifugation and selective lysis of RBCs.[4] On-chip separation and analysis of WBCs still face challenges.

For blood cell separation, many of the current microfluidic devices use physical fields under which heterogeneous cells have different mobilities. Dielectrophoretic-field-flow fractionation (DEP-FFF) isolates WBCs with a purity of 5% through balancing between DEP and sedimentation forces.[5] Magnetophoresis (MP) utilizes the different magnetic natures of blood cells for separation.[6,7] Immunomagnetic separation of WBCs has been demonstrated by selectively attaching magnetic beads to the cells.[8] Although they showed impressive results, their efficacy should be demonstrated without sample treatment such as media exchange and the adjustment of the ratio of WBCs to RBCs. In addition, the enrichment ratios of WBCs were not high enough for further analysis.

The difference in cell size and deformability is one of the criteria for separation of WBCs from RBCs. RBCs are smaller and more deformable than WBCs. The use of mechanical filters to isolate WBCs from RBCs has been demonstrated using silicon and poly(dimethylsiloxane) (PDMS) filter arrays.[9,10] The silicon filter array showed a RBC removal efficiency of 99.9% and was applied to on-chip polymerase chain reaction (PCR) of WBCs after separation. The filtration of WBCs in these static filter systems, however, was not conducted in a continuous manner and the amount of filtration samples is restricted to within the filter capacity. Also, it is not easy to recover the cells trapped in the filter after filtration. The deterministic bump arrays separated WBCs and RBCs continuously without clogging.[11] In this device, the enrichment of WBCs to RBCs was obtained up to 110-fold. A microfluidic device with a splitting and recombining channel network isolated WBCs in a continuous manner with an enrichment ratio of ~29 fold.[12] However, their dependence on a laminar stream makes it difficult to induce the dynamic movement of blood cells across the channel along field gradients as in the active methods. Therefore, it is necessary for cell separation to confine cells in a certain position of the fluid stream with sheath flow or to divide and re-distribute the fluid stream with complex channel networks. A microfabricated device for cross-flow filtration showed the RBC reduction ratio by a factor of ~4000 simultaneously exchanging the carrier medium.[13] However, it also depends on a complicated channel design to separate cells. Thus,

Department of Bio and Brain Engineering, Korea Advanced Institute of Science and Technology (KAIST), 335 Gwahangno, Yuseong-gu, Daejeon, 305-701, Republic of Korea. E-mail: jekyun@kaist.ac.kr; Fax: +82 42 869 4310; Tel: +82 42 869 4315

† Electronic supplementary information (ESI) available: Movie showing particle filtration. See DOI: 10.1039/b705203k

‡ The HTML version of this article has been enhanced with colour images.

it is essential to develop simple and efficient methods to isolate WBCs for easy integration with downstream analysis.

In this study, we present a novel hydrophoretic method for isolation of WBCs using a microfluidic device composed of slanted obstacles and filtration obstacles (Fig. 1). This device exploits the size and deformability difference between RBCs and WBCs. The filtration obstacles are designed with the same shape as the slanted obstacles, only shorter to create a filtration pore (Fig. 1(b)). Our previous works have demonstrated the movement of particles under the structure-induced pressure fields, which we call "hydrophoresis".[1,14] The slanted obstacles in a microchannel as the source of hydrophoresis were used to focus microparticles. Since the filtration obstacles have the same slanted structure as the slanted obstacles, they not only allow the passage of RBCs but also focus them to a sidewall by hydrophoresis. The slanted structure of the filtration obstacles also prevents trapping of WBCs into the gap in the obstacle area, allowing their continuous flow. This paper deals with the filtration of polystyrene particles with a minute diameter difference of 7.3% as the model for sphere particles. The focusing behaviors of small particles being able to pass the gap in the filtration obstacle area are explained with the pressure field simulation by computational fluid dynamics (CFD) software. Based on the difference of cell size, shape and deformability, WBCs were isolated from RBCs in the microfluidic device with the filtration obstacles.

Filtration principle

Fig. 1 illustrates overall focusing and filtering processes with schematic trajectories of the small and large particles passing the slanted obstacles and filtration obstacles. The slanted obstacles and filtration obstacles are formed on the bottom and top of a channel. The height of the slanted obstacles is higher than that of the filtration obstacles. In each process, the height and the gap of the obstacles are determined by the diameter of the particles to be separated. The first region for focusing consists of the slanted obstacles higher than the diameter of the particles to separate (Fig. 1(a)). The gap size between the obstacles and the top or bottom of the channel is also larger than the particles. Therefore, the small and large particles freely pass through the gap between the obstacle and the top or bottom of a channel without collision. The focusing principle is based on hydrophoresis utilizing microstructure-induced pressure fields.[1,14] The channel area around the slanted obstacle has less resistance to flow along the slanted obstacle than along the *y*-axis. The anisotropic fluidic resistance between the top- or bottom-area and side-areas of the obstacles generates lateral pressure gradients, which induce helical recirculation (see the curved arrows in Fig. 1(a)). The obstacle structure at the bottom and top generates helical recirculations in clockwise and counterclockwise directions, respectively. The fluid at the bottom or top of the slanted obstacles moves across the channel. Following the transverse flow along the *x*-axis, the particles are focused to a sidewall. In

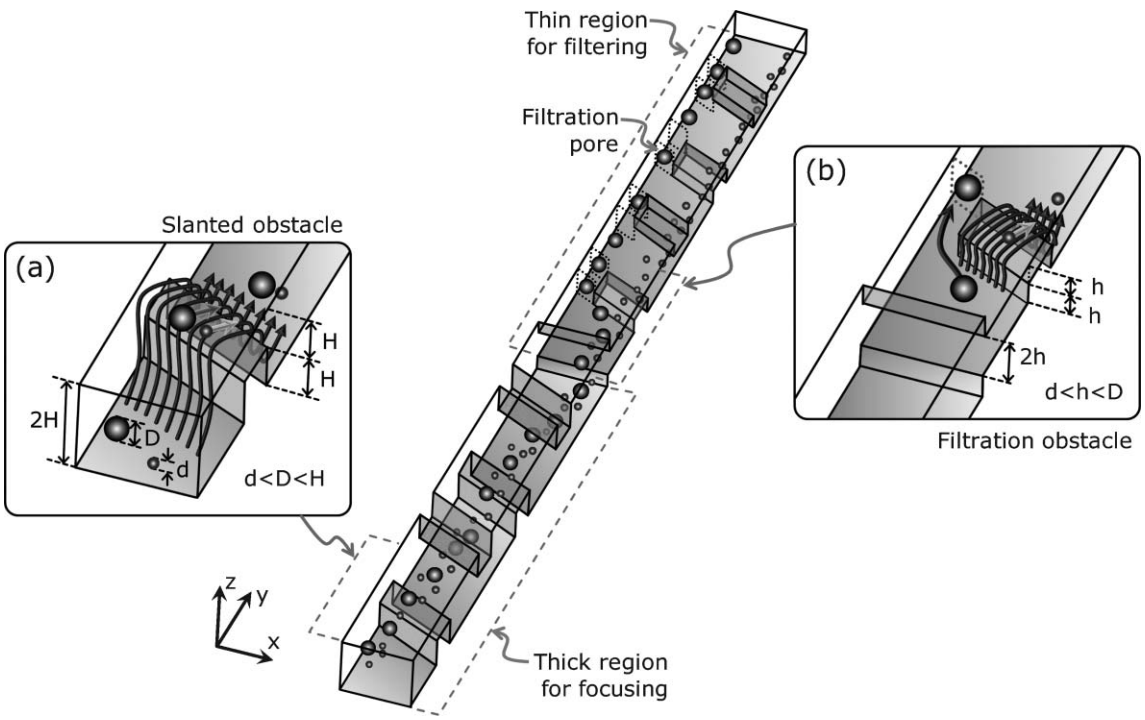

Fig. 1 Hydrophoretic filtration. The obstacles are alternately formed on the bottom and top of a channel. A flow direction is along the *y*-axis. (a) The slanted obstacles at the bottom and the top wall drive helical recirculation. Along the transverse flows, particles are focused to a sidewall. (b) In the filtering process, the gap between the filtration obstacle and the top or the bottom wall is set between the diameters of the small and the large particles. Therefore, the particle larger than the gap is blocked by the filtration obstacles and moves through the filtration pore. The smaller particle freely passes the gaps in the filtration obstacle areas and stays in its focused position.

the filtration process, the filtration obstacles form a filtration pore through which the large particle can pass (Fig. 1(b)). Also, the height of the filtration obstacle and the gap is set between the small and large particle diameters. Therefore, the particle smaller than the gap freely passes through it and keeps its focused position (focusing mode). In contrast, the particle larger than the gap collides against the obstacles and moves into the filtration pore (filtration mode). The height of the filtration obstacles in the filtering process defines the critical separation diameter.

Experimental

Design and fabrication of microfluidic device

The microfluidic device for hydrophoretic filtration is a stacked structure in which two poly(dimethylsiloxane) (PDMS)-channel layers with upper and lower obstacles face each other (Fig. 2(a)). Accordingly, the height of the obstacles and their gap were defined as half the channel height. The channel of the device consists of two regions with different channel heights. The first region for focusing has 20 slanted obstacles alternately formed on the bottom and top of the channel (1 of Fig. 2). The second region for filtering has 20 filtration obstacles with a filtration pore formed on the bottom and top of the channel (2 of Fig. 2). The height of the former channel region is higher than that of the latter one. The slanted obstacles in (1) of Fig. 2 were geometrically defined with W = 100 μm, Q = 70 μm, S = 210 μm, and $\theta = 55°$. The filtration obstacles in (2) of Fig. 2(b) had a filtration pore with the same geometry as the slanted obstacles. The width of the initial filtration pore gradually decreased to prevent channel clogging with particles. The width, D, of the filtration pore is 20 μm and its height is the same as the channel height. The whole channel was ~13 mm in length.

The device for hydrophoretic filtration was fabricated by two-step photolithography. The first spin-coating of PR (photoresist, SU8-2002 and −2010) defines filtration obstacles and the second coating determines slanted obstacles. Accordingly, the height of the slanted obstacles is higher than the filtration obstacles. For particle separation, the exact heights of filtration obstacles with 8.6 and 11.6 μm nominal heights were 8.55 ± 0.07 and 11.58 ± 0.02 μm, respectively. The filtration obstacles of 4.0 μm nominal height for blood cell separation were 3.92 ± 0.04 in exact height. The mixture of PDMS prepolymer and curing agent (Sylgard 184; Dow Corning, MI) in the ratio of 5 : 1 was poured on the PR mold and cured for ~3 h in a convection oven of 65 °C. To align and bond the PDMS replicas (one with upper obstacles and another with lower obstacles), after their brief treatment with oxygen plasma (200 mTorr, 200 W), we dipped them into ethyl alcohol solution. Since the oxidized surface of PDMS is preserved under liquid solutions, we could align and bond the PDMS replicas with each other.

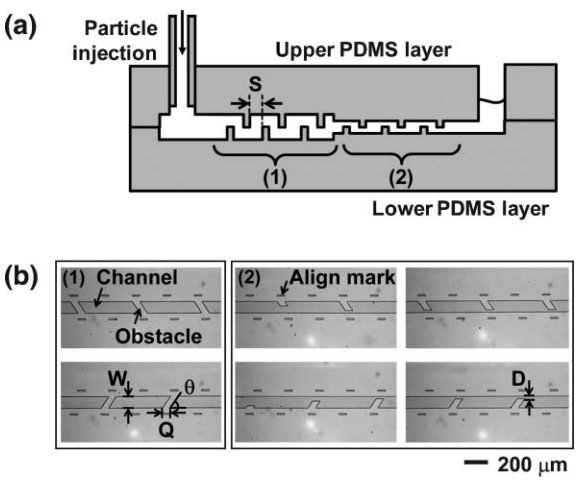

Fig. 2 Microfluidic device for hydrophoretic filtration. (a) Cross-sectional schematic diagram of the device after bonding. (b) Optical micrographs showing slanted obstacles and filtration obstacles before boding. A PDMS layer ((b) upper) with upper obstacles was bonded to another PDMS layer ((b) lower) with lower obstacles. The height of the slanted obstacles in (1) is higher than that of filtration obstacles in (2).

Preparation of polystyrene microspheres and blood cells

Plain polystyrene beads of 8, 9, 10, 11, and 12 μm nominal diameter (Sigma-Aldrich Co., MO) were used for the demonstration of hydrophoretic filtration. Their exact sizes were 8.02, 9.26, 10.09, 10.98, and 11.85 μm, respectively. They had coefficient of variation (CV) less than 2% for particle size. The beads were prepared in 0.2% Tween®20 aqueous buffer with concentrations of ~380, 260, 240, 250, and 150 μL^{-1} for 8 to 12 μm beads, respectively. As a surfactant, Tween®20 was used to minimize the hydrophobic interaction between a PDMS channel and a polystyrene bead, and beads.

For blood cell separation, Sprague-Dawley rat blood was drawn with EDTA or a mixture of EDTA and citrate as anticoagulant. Blood sample was used within 12 h of collection. We measured the size of blood cells through microscopic images. WBCs in suspension had a diameter in the range 4.1–7.9 μm (n = 20). RBCs in suspension had a diameter in the range 6.2–7.9 μm (n = 11) and a thickness in the range 1.7–2.6 μm (n = 6). WBCs in suspension are typically 6 to 10 μm in diameter.[15] When they are fixed to a glass slide to prepare a blood film, they can spread and become larger. To quantify separation efficiency, WBCs were stained with Hoechst (Invitrogen Co., CA), a nucleic acid-specific fluorescence dye. Since RBCs lack cell nuclei, they were not stained with the dye. WBCs were identified from RBCs by fluorescence.

Experimental setup

Bead mixtures or cells were introduced into the microfluidic device using a syringe pump (Pump 11 Pico Plus; Harvard Apparatus, Inc., MA). Particle images and videos were taken with a CCD camera (DS-2MBWc; Nikon Co., Japan) attached to an inverted optical microscope (TS100; Nikon Co.). The lateral position of particles was measured from images captured in the expanded outlet region of 1 mm. A commercial image analyzing program, i-Solution (iMTechnology Co., Korea) was used to measure particle positions, cell sizes, and the number of unstained RBCs and Hoechst stained WBCs. The images for measuring particle position were acquired at a resolution of 1024 × 768 pixels. In each experiment, more

than 100 particles were measured. Microparticle separation experiments were repeated four times. The pressure distributions in a microchannel were simulated using a commercial CFD solver (CFD-ACE+; CFD Research Co., Huntsville, AL).

Differential count of white blood cells

The differential counts of WBC subpopulations in initial and separated samples were performed using a hematology analyzer (Cell-dyn 3500; Abbott Laboratories, IL). The separated sample was mixed with phosphate buffered saline (PBS) in a minimum volume of $\sim$120 μL for the hematology analyzer.

Results and discussion

Particle movements passing through filtration obstacles

To demonstrate the hydrophoretic filtration, we tested whether particles larger than the gaps in the filtration obstacle areas can bump against the obstacles and change their flow direction. For this test, we individually injected microspheres with diameters of 11 and 12 μm into the microfluidic device, in which the heights of the slanted obstacles and filtration obstacles were 18.6 and 11.6 μm, respectively. In the device, the cross-sectional area of the filtration pore was 20 μm in width by 23.2 μm in height. The applied flow rate was 0.1 μL min^{-1}. Fig. 3(a) shows overlaid images of two different modes of separation. The time interval between particles in each image was 1/15 s. In the device with a critical separation diameter of 11.6 μm, the 11 μm bead stayed in its focused position (focusing mode), but the 12 μm bead collided against the 11.6 μm-height filtration obstacles and passed through the filtration pore (filtration mode). During the experiment, we observed the local trapping of particles in the gap between the filtration obstacles and the top or bottom of the channel due to the small difference in the size between the gap and particles, $\sim$500 nm. However, there was no severe clogging due to the gradual decrease of the initial filtration pore as shown in (2) of Fig. 2(b). Also, as live eukaryotic cells are deformable, the trapping of cells was not observed in blood cell separation.

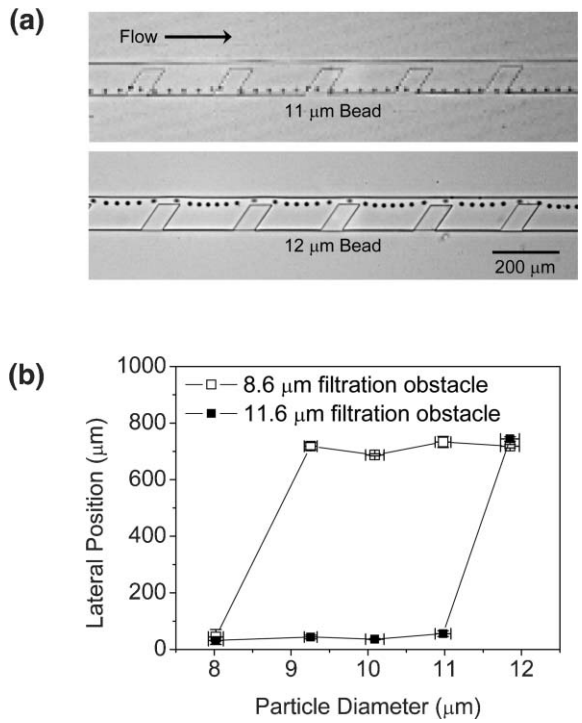

Fig. 3 (a) Optical micrographs showing trajectories of 11 and 12 μm beads passing the 11.6 μm filtration obstacles at 0.1 μL min^{-1}. (b) Lateral position of particles as a function of microsphere diameters, measured in the expanded outlet region of 1 mm. Microbeads ranging from 8 to 12 μm diameter were injected into two microfluidic devices with different heights of filtration obstacles; 8.6 and 11.6 μm, respectively. The applied flow rate was 2 μL min^{-1}.

The transition of the separation modes was then characterized with several beads ranging from 8 to 12 μm in diameter. The microfluidic devices were designed for two-different types; one had 16.2 μm-height slanted obstacles and 8.6 μm-height filtration obstacles, and the other had 18.6 μm-height slanted obstacles and 11.6 μm-height filtration obstacles. In the device with 8.6 μm-height filtration obstacles, the cross-sectional area of the filtration pore was 20 μm in width by 17.1 μm in height. The particles were individually injected into the microfluidic devices at 2 μL min^{-1}. On a given critical separation diameter, particles with smaller diameters than the criterion value took the focusing mode, and particles with larger diameters took the filtration mode (Fig. 3(b)). In the device with 8.6 μm-height filtration obstacles, only 8 μm beads flowed in the lateral range of 44.2 $\pm$ 26.4 μm (focusing mode). In contrast, only 12 μm beads flowed in the range of 744.2 $\pm$ 7.8 μm in the device with 11.6 μm-height filtration obstacles (filtration mode). In our previous study, particles having a comparable size to the slanted obstacles were aligned to the center of the channel height and exposed to an identical pressure field. Therefore, they flowed to the same lateral region.[1] In the same way, 8 to 11 μm-sized particles were completely focused to a sidewall within the range 31.7–56.0 μm in the device with 11.6 μm-height filtration obstacles. The advantage of the filtration obstacles over conventional filters is that they play not only the role of filtering large particles but also the role of focusing small particles able to pass through the gap in the obstacle area. Therefore, through hydrophoretic filtration, the desired target can be completely separated by size from unnecessary elements.

Pressure fields around filtration obstacles

By applying a pressure drop across the simulation geometry with filtration obstacles and the filtration pore, we obtained pressure fields and velocity vectors, which lead to transverse motions of a microparticle. The geometric conditions were identical with the experimental ones in Fig. 3(a). The applied flow rate was 0.1 μL min^{-1} along the y-axis. The values of the field intensity in each cross-section were normalized for clear illustration. Fig. 4 shows the variation of the pressure field intensity generated by the filtration obstacles. The insets are the enlarged views of the projected velocity vectors around the lower filtration obstacle. The pressure field intensity is higher at the filtration pore and it becomes lower going to the right sidewall. There are no significant variations of the field

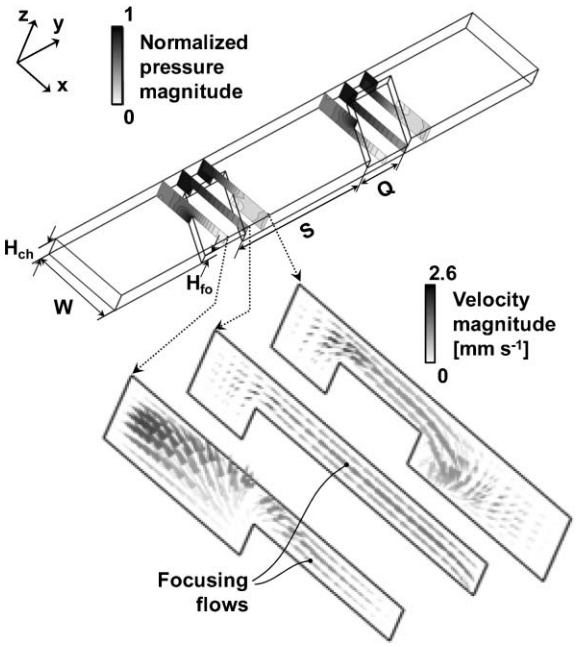

Fig. 4 Simulated pressure fields. The simulation geometry composed of lower and upper filtration obstacles and the cross-sectional plots of pressure distributions at an applied flow rate of 0.1 μL min^{-1}. The enlarged plots describe the projected velocity vectors to the cross-sectional surfaces.

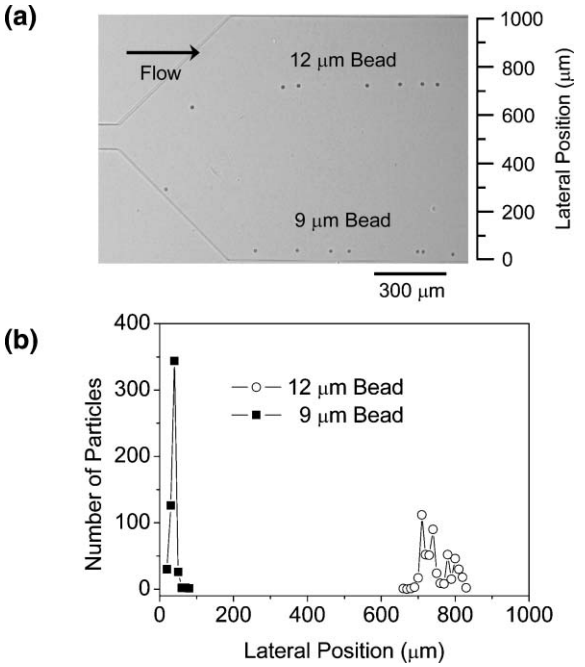

Fig. 5 (a) Optical micrograph showing separated particle positions. (b) Measured profiles of the beads with 9 and 12 μm diameters at a flow rate of 1 μL min^{-1}. In this experiment, the height of filtration obstacles was 11.6 μm as a critical separation diameter. The beads were identified by size difference.

intensity in the filtration pore. The pressure field gradient from the left to the right sidewall drives the focusing flows (see the insets of Fig. 4). The lateral flow induced by the transverse pressure gradient focuses small particles, which can pass through the gaps in the obstacle areas, to the right sidewall. On the other hand, large particles, which bump against the obstacles, move to the filtration pore. As shown in Fig. 3(a), the 11 μm particle smaller than the gap of 11.6 μm in height was completely focused to the sidewall.

The alternate placement of slanted obstacles on the bottom and top of a channel plays an important role in hydrophoretic filtration. Slanted obstacles only at the bottom of the channel generated clockwise rotational flows, in which particles move back and forth between one sidewall and the other sidewall.[1] The conventional filtration methods having filters perpendicular to an applied flow have an isotropic fluidic resistance in their channels and do not require the relatively complex arrangement of their filters on the top and bottom of a channel. However, the advantage of the focusing function of our filtration obstacles outweighs the complex arrangement of the obstacles. Without the focusing of particles, filtration methods can have wide separation bands, which will lower their separation efficiency.

Hydrophoretic filtration of microparticles

Using the device with 11.6 μm-height filtration obstacles, we completely separated mixed particles of 9 and 12 μm beads. The applied flow rate for separation was 1 μL min^{-1}. Consequently, the lateral position of separated particles (Fig. 5) corresponds well to the individually measured data of Fig. 3(b) (See ESI video †). The 9 and 12 μm beads took the focusing and filtration mode, respectively. Applying the resolution equation of separation in chromatographic analysis,[16] we could get a separation resolution of 6.2 for the hydrophoretic filtration.

$$R = \frac{2\Delta D}{(\sigma_1 + \sigma_2)} \quad (1)$$

where R is the separation resolution, ΔD is the distance between the peaks of any two separands, and σ_1 and σ_2 are the respective peak widths of the separands. Compared with our previous separation method based hydrophoresis,[1] the separation resolutions increased by 6.4-fold.

Interactions between particles can affect the separation purity, such as the pearl-chain interaction between polarized particles and non-specific agglomeration of particles.[17,18] Therefore, microfluidic separation methods typically adopted multiple rounds of separation to improve separation purity[19] or showed low separation purity in a single round of separation.[5] During the hydrophoretic filtration, 12 μm beads larger than the gap in the filtration obstacle area cross the separation channel from the focused position to the filtration pore. Their crossing can disturb the focusing mode of 9 μm beads. However, the filtration obstacles serve to focus the small particles as well as to filtrate the large particles. Therefore, the disturbance by the crossing of 12 μm was negligible for the particle separation.

Hydrophoretic filtration of blood cells

Applying the hydrophoretic filtration method, we isolated WBCs from RBCs. The microfluidic device was designed with

slanted obstacles of 13.0 μm height and filtration obstacles of 4.0 μm height. In the device, the cross-sectional area of the filtration pore was 20 μm width by 7.8 μm height. The channel of the device was equally divided into two outlets; one for WBCs and another for RBCs (Fig. 6(a)). The applied flow rate for blood cell separation was 1 μL min^{-1}. The concentration of blood cells was $\sim 5 \times 10^9$ cells mL^{-1} and WBCs occupied 0.28% of the total cells. The blood sample was diluted 1 : 20 in PBS buffer for this separation experiment. Erythrocytes have a biconcave disk shape, and their diameters are 6.2–7.9 μm, a similar size to that of leukocytes. Therefore, it can be difficult to separate two cell types based on their sizes. However, RBCs are easily deformed due to their large surface area to volume[20] and thereby pass through small capillaries even with a diameter of ~3 μm. In our device, RBCs were aligned parallel to the filtration obstacles of 4.0 μm-height due to their small thickness of 1.7–2.6 μm and deformability. The majority of RBCs chose the focusing mode. Conventional filters have exploited the degree of RBC deformability to quantify RBC damage.[21,22] In our device, a decrease of RBC deformability can make RBCs difficult to pass through the gap in the filtration obstacle area. Impaired RBCs would take the filtration mode. By the filtration process, WBCs were isolated with a purity of ~58% (710 WBCs in 1221 total cells) at a throughput of 4×10^3 cells s^{-1} (Fig. 6(b) and (c)). Up to 85% of WBCs were recovered compared with their initial concentration. Our hydrophoretic filtration device enriched WBCs to ~210-fold from RBCs in just a single round of separation. As

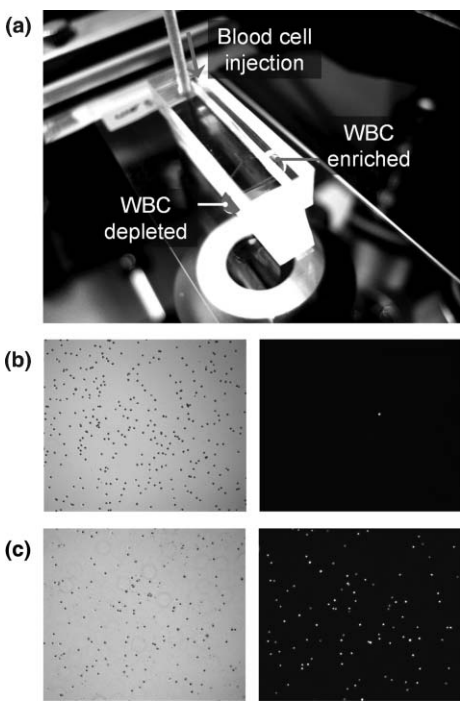

Fig. 6 (a) Blood cell separation. WBCs and RBCs were separated following the filtration and the focusing mode, respectively. The critical separation diameter of 4.0 μm set between the thickness of RBCs and the diameter of WBCs. (b), (c) Blood cells before separation (b) and after separation (c) are shown in bright-field (left) and fluorescence (right) images. These images were acquired with 50× magnification.

mentioned before, because of deformability of the cells, cell trapping between the filtration obstacles and the top or bottom of a channel was not observed. However, the deformability of WBCs can have a negative effect on their recovery. Since WBCs with diameters between 4 and 5 μm can deform within a gap of 4 μm height, they would pass through the gap in the filtration obstacle area in the focusing mode and decrease the recovered number of WBCs at the outlet for WBCs. The simplest way to increase the recovery ratio of WBCs is to reduce the gap size between the filtration obstacles and the top or the bottom of a channel. In the device with a gap of 3 μm height, most deformed WBCs will be blocked by the filtration obstacles and RBCs with thicknesses of 1.7–2.6 μm will pass through the gaps in the focusing mode.

Recovery of white blood cells and their subpopulations

We also tested the hydrophoretic filtration device to quantify the differential recovery of WBCs as well as their total recovery. The concentration of blood cells used in this experiment was $\sim 6.4 \times 10^9$ cells mL^{-1}. The concentration of WBCs in the blood was $\sim 1.1 \times 10^7$ cells mL^{-1}, which was composed of neutrophils (13.3%), lymphocytes (69.3%), monocytes (5.2%), eosinophils (0.4%), and basophils (11.7%). The blood sample was diluted 1 : 10 in PBS buffer for this separation experiment. The applied flow rate for blood cell separation was 1 μL min^{-1}. Blood was run through the filtration device over 1 h. The filtrated sample was collected and counted by a conventional hematology analyzer. The principal leukocytes of a rat are neutrophils and lymphocytes. The differential count of the other cells such as monocytes, eosinophils, and basophils show high coefficients of variation (CVs) of 40–50% due to their lower absolute numbers.[23,24] Therefore, we could obtain reliable recovery rates only for neutrophils and lymphocytes. After the hydrophoretic filtration, neutrophils and lymphocytes were recovered up to 75 and 70%, respectively, compared with their initial concentrations. The total recovery rate for two cell types was ~71%. There is no significant difference in the recovery rate between the WBC subpopulations. The recovered cells can be used for correlation studies between certain diseases and global gene expression changes in leukocytes.[25]

The relative and absolute populations of WBC types are important parameters for diagnosis of viral infectious diseases, monitoring of malignant disease such as leukemia, and staging of human immunodeficiency virus (HIV) infection. Increased number of lymphocytes can be associated with mononucleosis usually caused by the Epstein–Barr virus (EBV).[26] Chemotherapy, radiation treatment, and some cancers may cause neutropenia, a hematological disorder with decreased number of neutrophils.[27] HIV infection can result in low numbers of circulating lymphocytes.[28]

The hydrophoretic filtration method exploits differences in size and deformability of cells as the principle of filtration. The size range of each WBC subpopulation used for the separation experiment overlap with each other. There is no significant difference in size between WBC subpopulations.[15] Therefore, it is difficult to isolate target WBC subpopulation only by size. The most widely used methods for the differential

separation of WBC subpopulations are magnetic-activated cell sorting (MACS) and fluorescence-activated cell sorting (FACS).[29–31] In these methods, monoclonal antibodies tagged with magnetic or fluorescent compounds are used to separate cells based on their specific antigenic determinants. To isolate specific WBC subpopulations, our hydrophoretic filtration method can adopt a strategy similar to MACS or FACS in labelling cells with microparticles. The size of the cells tagged with microparticles will increase significantly and be isolated from the unlabeled ones. The isolated cells can provide clinically useful information for the above-mentioned diseases.

Conclusions

We have proposed a new hydrophoretic filtration method using slanted obstacles and filtration obstacles. The filtration obstacles as a filter play not only the role of filtering large particles blocked by the obstacles but also the role of focusing small particles able to pass through the gap in the obstacle area. Therefore, we can separate microparticles by size in a binary manner, sorting the desired target from unnecessary elements. From the experimental results, we showed that particles with a minute diameter difference of 7.3% were completely separated through hydrophoretic filtration. The critical separation diameter can be easily defined by changing the height and gap of the filtration obstacle. By applying hydrophoretic filtration, a wide range of particles can be separated by size in a binary manner. In the presented device, we separated WBCs from RBCs with an enrichment ratio of $\sim$210-fold at a throughput of 4×10^3 s^{-1}. A filtration time of $\sim$0.3 s can minimize cell damage from shear stress. Adding the focusing process, the whole process time was $\sim$1.3 s. The current design of the device can separate particles into two groups: one group smaller than the critical separation diameter and the other group larger than the criterion. The filtration device has a simple channel design and can be fabricated using rapid prototyping. This will enable extension to the device with multiple heights and the separation of particles with multiple diameters, individually.

Acknowledgements

This research was supported by the Nano/Bio Science & Technology Programs (M10536090002-05N3609-00210) of the Ministry of Science and Technology (MOST), Korea. We acknowledge the Chung Moon Soul Center for BioInformation and BioElectronics, KAIST. The microfabrication work was performed at the Digital Nanolocomotion Center. We thank Dr Chul-Ho Lee for his help with the hematology analyzer.

References

1 S. Choi and J.-K. Park, *Lab Chip*, 2007, **7**, 890.
2 M. Toner and D. Irimia, *Annu. Rev. Biomed. Eng.*, 2005, **7**, 77.
3 A. J. Tüdős, G. A. J. Besselink and R. B. M. Schasfoort, *Lab Chip*, 2001, **1**, 83.
4 E. Verpoorte, *Electrophoresis*, 2002, **23**, 677.
5 X.-B. Wang, J. Yang, Y. Huang, J. Vykoukal, F. F. Becker and P. R. C. Gascoyne, *Anal. Chem.*, 2000, **72**, 832.
6 K.-H. Han and A. B. Frazier, *J Microelectromech. Syst.*, 2005, **14**, 1422.
7 K.-H. Han and A. B. Frazier, *Lab Chip*, 2006, **6**, 265.
8 D. W. Inglis, R. Riehn, R. H. Austin and J. C. Sturm, *Appl. Phys. Lett.*, 2004, **85**, 5093.
9 P. Wilding, L. J. Kricka, J. Cheng, G. Hvichia, M. A. Shoffner and P. Fortina, *Anal. Biochem.*, 1998, **257**, 95.
10 H. Mohamed, L. D. McCurdy, D. H. Szarowski, S. Duva, J. N. Turner and M. Caggana, *IEEE Trans Nanobiosci.*, 2004, **3**, 251.
11 J. A. Davis, D. W. Inglis, K. J. Morton, D. A. Lawrence, L. R. Huang, S. Y. Chou, J. C. Sturm and R. H. Austin, *Proc. Natl. Acad. Sci. U. S. A.*, 2006, **103**, 14779.
12 M. Yamada and M. Seki, *Lab Chip*, 2005, **5**, 1233.
13 V. VanDelinder and A. Groisman, *Anal. Chem.*, 2007, **79**, 2023.
14 S. Choi and J.-K. Park, *Proc. Micro Total Analysis Systems 2006 Conference*, Tokyo, Japan, 2006, pp. 371–373.
15 P. Sethu, A. Sin and M. Toner, *Lab Chip*, 2006, **6**, 83.
16 D. A. Skoog, F. J. Holler and T. A. Nieman, *Principles of instrumental analysis*, 5th edn, Thomson Learning, London, UK, 1998, p. 688.
17 S. Choi and J.-K. Park, *Lab Chip*, 2005, **5**, 1161.
18 N. Pamme and A. Manz, *Anal. Chem.*, 2004, **76**, 7250.
19 X. Hu, P. H. Bessette, J. Qian, C. D. Meinhart, P. S. Daugherty and H. T. Soh, *Proc. Natl. Acad. Sci. U. S. A.*, 2005, **102**, 15757.
20 H. Noguchi and G. Gompper, *Proc. Natl. Acad. Sci. U. S. A.*, 2005, **102**, 14159.
21 R. E. Waugh, *Blood*, 1991, **78**, 3037.
22 S. S. Shevkoplyas, T. Yoshida, S. C. Gifford and M. W. Bitensky, *Lab Chip*, 2006, **6**, 914.
23 E. W. Thewlis and O. O. Meyer, *Anat. Rec.*, 1942, **82**, 115.
24 J. Kieffer, G. Winkler, L. V. Hove, A. Walsh, P. Thomann, S. Wyss, E. Eggenberger and H. Lutz, *Comp. Haematol. Int.*, 1999, **9**, 92.
25 P. Sethu, L. L. Moldawer, M. N. Mindrinos, P. O. Scumpia, C. L. Tannahill, J. Wilhelmy, P. A. Efron, B. H. Brownstein, R. G. Tompkins and M. Toner, *Anal. Chem.*, 2006, **78**, 5453.
26 V. V. Novitskii, O. I. Urazova, I. O. Nasledni kova, A. P. Pomogaeva and L. V. Syusina, *Bull. Exp. Biol. Med.*, 2002, **134**, 57.
27 T. W. Kuijpers, R. S. Weening and D. Roos, *J. Immunol. Methods*, 1999, **232**, 211.
28 X. Cheng, D. Irimia, M. Dixon, K. Sekine, U. Demirci, L. Zamir, R. G. Tompkins, W. Rodriguez and M. Toner, *Lab Chip*, 2007, **7**, 170.
29 L. Sun, M. Zborowski, L. R. Moore and J. J. Chalmers, *Cytometry*, 1998, **33**, 469.
30 M. Berger, J. Castelino, R. Huang, M. Shah and R. H. Austin, *Electrophoresis*, 2001, **22**, 3883.
31 L. A. Herzenberg, D. Parks, B. Sahaf, O. Perez, M. Roederer and L. A. Herzenberg, *Clin. Chem.*, 2002, **48**, 1819.

